First principles calculations of the electronic and geometric structure of $Ag_{27}Cu_7$nanoalloy

Marisol Alcántara Ortigoza* and Talat S. Rahman†
Department of Physics, University of Central Florida, Orlando, Florida 32816-2385, USA
(Received 14 December 2007; revised manuscript received 20 February 2008; published 5 May 2008)

Ab initio calculations of the structure and electronic density of states (DOS) of the perfect core-shell $Ag_{27}Cu_7$ nanoalloy attest to its D_{5h} symmetry and confirm that it has only six nonequivalent (two Cu and four Ag) atoms. The analyses of bond length, average formation energy, and heat of formation of $Ag_{27}Cu_7$ and $L1_2$ bulk Ag-Cu alloys provide an explanation for the relative stability of the former with respect to the other nanoalloys in the same family. The highest occupied molecular orbital–lowest unoccupied molecular orbital gap is found to be 0.77 eV, which is in agreement with previous results. The analyses of the DOS of $Ag_{27}Cu_7$, $L1_2$ Ag-Cu alloys, and related systems provide insight into the effects of low coordination, contraction or expansion, and the presence of foreign atoms on the DOS of Cu and Ag. While some characteristics of the DOS are reminiscent of those of the phonon-stable $L1_2$ Ag-Cu alloys, the Cu and Ag states hybridize significantly in $Ag_{27}Cu_7$, compensating for the *d*-band narrowing that each atom undergoes and hindering the dip in the DOS found in the bulk alloys. Charge density plots of $Ag_{27}Cu_7$ provide further insight into the relative strengths of the various interatomic bonds. Our results for the electronic and geometric structures of this nanoalloy can be explained in terms of length and strength hierarchies of the bonds, which may have implications also for the stability of alloys in any phase or size.

DOI: 10.1103/PhysRevB.77.195404 PACS number(s): 61.46.−w, 73.22.−f, 63.20.−e, 71.20.Be

I. INTRODUCTION

Small bimetallic nanoclusters often have physical and chemical properties that are distinct from those of their pure bulk counterparts and suggestive of novel applications.[1–3] Not surprisingly, materials assembled from finite-sized bimetallic clusters have been investigated intensively not only for their catalytic and optical properties[4–14] but also for their ability to assemble into *cluster crystals*[15,16] and their possible applications in single-electron tunneling devices.[1] Along with its high symmetry and relatively high melting temperature, one of the criteria for a cluster to be used as a potential building block for cluster-assembled materials is its chemical stability relative to other reagents and to other clusters of the same material. Also, major difficulties arise from the fact that clusters may tend to coalesce when assembled. This can be prevented in one of two ways—either by isolating the clusters in matrices or by coating them with surfactants.[16] An alternative route is to find nanoclusters that are naturally stable, i.e., nanoclusters whose intracluster interaction is stronger than the intercluster interaction, allowing the clusters to keep their individual identity intact upon assembling. Even so, cluster-assembled materials could still be metastable against dissociation into their bulk phases.

Darby *et al.*,[3] using many-body Gupta potentials, studied the structure and stability (as reflected by the total energy) of a wide variety of Cu_xAu_y nanoclusters with up to 56 atoms and $x/y=1$ and 3, corresponding to the well-known $x:y$ ratios that result in stable ordered bulk phases at low temperatures.[17] They found that the geometry of the cluster is influenced by the tendency to maximize the number of Cu-Au and Au-Au bonds. Rossi *et al.*,[1] on the other hand, proposed a new family of 34-atom bimetallic alloys by using the genetic global optimization (GGO) technique.[1] These nanoalloys are characterized by a perfect core-shell structure in which the *smaller* atoms (Cu or Ni) compose the core, whereas the relatively larger Ag atoms lie on the surface. They found the nanoalloys to be energetically and thermodynamically more stable than pure clusters Ni_{34}, Cu_{34}, and Ag_{34} (Ref. 1) and attributed the relative stability of the nanoalloy structures to the supplanting of the inner Ag atoms by *smaller* atoms (Cu or Ni), therefore reducing the internal strain in Ag_{34}, or the replacement of outer Cu atoms by *larger* atoms (Ag) to reduce the external strain in Cu_{34}. As we shall see later, the most stable of the 34-atom Ag-Cu nanoalloy family proposed by Rossi *et al.*[1] $Ag_{27}Cu_7$, provides a hint that it is not the $x:y$ ratio that guarantees the stability of either bulk or nanoalloys, rather, it is the maximization of the number of *optimized* Cu-Cu and Cu-Ag bonds.

Among a set of possible core-shell nanoclusters modeled by many-body interatomic potentials, Rossi *et al.*[1] chose the compositions corresponding to their most stable structures for some selected sizes and *locally* optimized the structures by using density functional theory (DFT) to confirm the trends given by the GGO and to single out the clusters with high electronic stability, namely, with the largest width of highest occupied molecular orbital–lowest unoccupied molecular orbital (HOMO-LUMO) gap. They determined the thermodynamic stability of the chosen structures through calculations of the melting temperatures from molecular dynamics simulations and of temperature-dependent probabilities of the global minima by harmonic thermodynamics.[18] Among the 34-atom family of nanoclusters, they found $Ag_{27}Cu_7$ and $Ag_{27}Ni_7$ to have the least excess energy with respect to bulk atoms (the lowest heat of formation), strong electronic stability (large HOMO-LUMO gap), and relatively high melting temperatures.[1] For these compositions, the GGO method finds the lowest energy structure to have D_{5h} symmetry, in which the 7 core-Cu atoms form a decahedron, while the 27 shell-Ag atoms are placed in an anti-Mackay overlayer. In general, the formation of nanoclusters is driven by the tendency to minimize dangling bonds.[1] Even though

such a tendency would lead to spherical structures,[1] the presence of d states increases the tendency to create directional bonding (s-d hybridization), which is manifested by the preference for well-ordered atomic structures, such as the decahedral forms.[19]

Experiments and heat of formation calculations have shown that Ag-Cu alloys generally tend to segregate.[20–22] In a sense, the core-shell structure of $Ag_{27}Cu_7$ nanoalloy is itself segregated. In order to understand how its particular geometry implicitly stabilizes it, a detailed examination of the relative strengths and lengths of the Ag-Cu, Cu-Cu, and Ag-Ag bonds is needed. For bulk Cu-Au alloys, the presence of a dip in the electronic density of states (DOS) near the Fermi level was also considered to be a signature of alloy stability.[20] Interestingly, such a dip is not found in bulk Au-Ag alloys.[17,20] Moreover, in the case of crystalline solids, the structural stability is linked to the absence of phonon instabilities.[23] The purpose of this paper is to carry out a full investigation of the relationship between the geometric and electronic structures of the $Ag_{27}Cu_7$ nanoalloy and related bulk systems to get insights into the various factors that may impact their stability. That is, through the examination of the formation energy, the density of states near the Fermi level, the HOMO-LUMO gap, and the charge density distribution, we develop criteria which may lead to chemical and electronic stability of $Ag_{27}Cu_7$. To obtain additional insights into the structure-stability relationship, we have also carried out calculations of the bond length, the electronic structure, and the phonon dispersion of Ag_3Cu and Cu_3Ag bulk alloys in their $L1_2$ phase.[24]

The rest of the paper is organized as follows: Section II contains the computational details, while Sec. III is a summary of our results. Section III A analyzes the geometry and bond coordination of the atoms in the $Ag_{27}Cu_7$ nanoalloy and those in the bulk Ag-Cu Ll_2 alloys, for insights into the proposed stability criteria. In Sec. III B, we examine our calculated DOS of $Ag_{27}Cu_7$ and of the bulk systems (Cu_3Ag and Ag_3Cu), and the charge density distribution of $Ag_{27}Cu_7$. Finally, in Sec. IV, we summarize our conclusions and discuss how the relationship between structure and stability in $Ag_{27}Cu_7$ nanoalloy can be understood in terms of a specific hierarchy in bond strength and the capability of the structure to provide the bond lengths for which that hierarchy is satisfied.

II. COMPUTATIONAL DETAILS

Periodic supercell calculations are performed in the framework of density functional theory.[25] Our calculations are based on the pseudopotential approach and the plane wave method (Quantum ESPRESSO: opEn-Source Package for Research in Electronic Structure, Simulation, and Optimization).[26] We use ultrasoft pseudopotentials[27] with the generalized gradient approximation for the exchange-correlation functional as provided by the Perdew-Burke–Ernzerhof expression.[28]Integrations up to the Fermi surface are performed by using a broadening technique[29] with a smearing parameter of 0.2 eV (0.147 Ry). Below we provide some specifics of the calculations as relevant to a particular system.

A. Calculation of bulk systems

We have performed extensive convergence tests for lattice constants, bulk moduli, and total energies of bulk Cu, Ag, Ag_3Cu, and Cu_3Ag. To obtain the minimum energy configuration with zero stress based on total energy differences of 1 mRy, as well as convergence up to the third and second digits in the lattice parameter (in a.u.), and the bulk modulus (in Mbar), respectively, the calculations demand a k-point sampling of 145 Monkhorst–Pack special points[30] (corresponding to a $16\times16\times16$ Monkhorst–Pack grid) for the integrations over the Brillouin zone (BZ). Furthermore, the plane wave kinetic energy cutoff, E_{cut}, and the energy at which the charge density Fourier expansion is truncated, E_ρ, had to be set equal to 680 eV (50 Ry) and 8160 eV (600 Ry), respectively. These convergence criteria surpass by far most of those reported in the literature, but are necessary to obtain reliable results in the present case, as we will see.

The lattice dynamics of Ag_3Cu and Cu_3Ag bulk alloys at arbitrary wave vectors is obtained by the perturbational DFT (DFPT), which is based on the linear response theory.[31–33] To determine the force constants, we use a $2\times2\times2$ q-point mesh in the BZ of the Ll_2 structure.[32] Phonon dispersion curves are obtained by the standard Fourier interpolation method.[32]

B. Calculation of $Ag_{27}Cu_7$ nanoalloy and isolated atoms

Since in the unrelaxed configuration of $Ag_{27}Cu_7$ the separation between the most distant atoms is about 8.7 Å, we locate the alloy inside a cubic supercell with a side length of 24 Å. In this manner, we ensure that as a result of periodic boundary conditions, the atoms at the edges of neighboring clusters are at least 15 Å apart, thereby isolating the clusters from each other. The same cubic box is used to model and calculate the total energy of isolated Cu and Ag atoms, using a spin-polarized calculation.

In this work, the Broyden–Fletcher–Goldfarb–Shanno algorithm[34] is used to minimize the nanoalloy total energy as a function of atomic positions.[26] At equilibrium, forces on the nanocluster atoms are required to be below 6.5×10^{-4} eV/Å (2.6×10^{-5} Ry/a.u.). Given the large separation between nanoclusters (isolated atoms) in neighboring supercells, integrations over the BZ using only one k point lead to reliable convergence in the calculated values of the total energy (see Ref. 35). For the nanoalloy, E_{cut} and E_ρ are 680 and 8160 eV, respectively, as mentioned above. Since these parameters surpass the demands for convergence in other systems involving copper or silver, and using the same DFT code,[36,37] we expect them to work well for the nanoalloys of interest here. While these demands for convergence make the calculations very CPU intensive, it is worth mentioning that we find the total energy and even the geometry of the nanoalloy to be severely affected if we were to use the default values of $E_{cut}=340$ eV and $E_\rho=1360$ eV in the code. For example, with the latter choice, the fully relaxed D_{5h} structure (resulting from $E_{cut}=680$ eV and $E_\rho=8160$ eV) is no longer stable and relaxes toward a structure in which the atomic positions break the D_{5h} symmetry by displacements

of up to 1 Å from their original positions and forces cannot be lowered below 2.5×10^{-2} eV/Å.

III. RESULTS AND DISCUSSION

Since the nanoalloy presents several opportunities for comparison of its properties and development of criteria for its stability, we find it beneficial to divide this section into two subsections, each of which consists of several parts. In Sec. III A, we concentrate on issues related to the geometry, the distribution of bond lengths, the atomic coordination, and the formation energy of the nanoalloy. We first introduce a notation in Sec. III A 1 that classifies the atoms in $Ag_{27}Cu_7$ according to their location within the nanoalloy. In Sec. III A 2, we inspect how the local coordination of the atoms in the nanoalloy relates to the bond lengths. Since there is hardly any experimental data on $Ag_{27}Cu_7$ and since the calculations of the phonon density of states of the nanoalloy from first principles are still a challenge, we have included in Sec. III A 3 our results for the structure and dynamics of bulk alloys, Ag_3Cu and Cu_3Ag, to gain insights and draw stability criteria for the nanoalloy of interest here. The average formation energy of the $Ag_{27}Cu_7$ nanoalloy and the stability considerations are analyzed in Sec. III A 4.

In Sec. III B, we focus on the electronic DOS and the local charge density of the nanoalloy. Section III B 1 contains the electronic DOS of the $Ag_{27}Cu_7$ nanoalloy and includes for comparison also those of bulk alloys, Ag_3Cu and Cu_3Ag. The local charge density distribution in the nanoalloy is summarized in Sec. III B 2.

A. Geometry, bond coordination, and stability considerations

1. Geometric structure of $Ag_{27}Cu_7$ nanoalloy

The initial configuration we adopted for the $Ag_{27}Cu_7$ nanoalloy[38] nicely relaxes toward the D_{5h} symmetry after energy minimization, as seen from the plots in Fig. 1. Accordingly, there are only six types of nonequivalent atoms: four types of Ag and two types of Cu atoms. This leads to a natural and useful classification of the atoms that refers to their distance from the mirror plane: Cu layer 0 (Cu0), Ag layer 0 (Ag0), Cu layers ±1 (Cu1), Ag layers ±2 (Ag2), Ag layers ±3 (Ag3), and Ag layers ±4 (Ag 4), as shown in Fig. 1. Layer 0, which lies on the mirror plane, consists of two pentagonal structures: the smaller one is made of copper atoms (Cu0) and fits in the larger one that is composed of silver atoms (Ag0) [Figs. 1(a) and 1(b)]. The *single-atom layers*, layers ±1 and ±4, sit on the fivefold rotation axis [see Figs. 1(c) and 1(f)]. The other two pentagonal layers, ±2 and ±3, are centered at the fivefold symmetry axis [Figs. 1(d) and 1(e)]. The radii of Ag2 and Cu0 pentagons are parallel to each other, but rotated 36° with respect to the Ag0 and Ag3 pentagons, as shown in Fig. 2. Since the layers are symmetric with respect to a mirror plane, the cluster can be characterized by only five of them, say, the central layer (layer 0) and those above this (layers 1–4). Ultimately, the symmetry of $Ag_{27}Cu_7$ allows us to fully describe its geometric structure by using eight parameters: the interlayer distances (d_{01}=1.341 Å, d_{12}=0.052 Å, d_{23}=0.992 Å, and d_{34}=1.512 Å) and the pentagon side lengths (a_{Cu0}=2.584 Å, a_{Ag0}=4.897 Å, a_{Ag2}=5.115 Å, and a_{Ag3}=2.948 Å, as shown in Fig. 2). The dislocations in the D_{5h} structure, as present in our initial configuration,[38] relaxed into the perfect D_{5h} structure under the stringent criterion that the apothem of each pentagon can be well defined up to 0.0003 Å, while interlayer distances are well defined up to 0.0001 Å. The interatomic bond lengths for the 34 atoms in the cluster, in the relaxed geometry, are summarized in Table I and discussed in detail below.

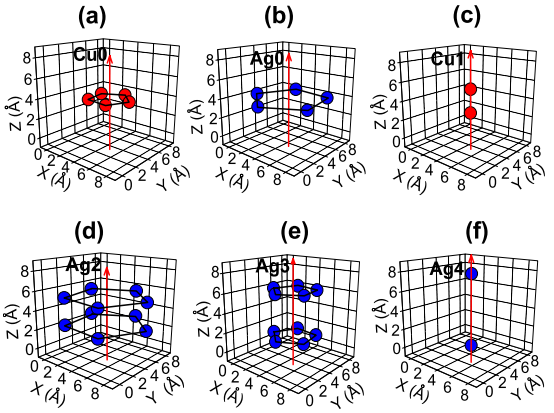

FIG. 1. (Color online) Three-dimensional picture of the six types of nonequivalent atoms. The vertical arrow represents the five-fold rotation axis. (a) Five Cu0 atoms sitting on the mirror plane of the cluster (z_0=3.88 Å). Note that the z_i coordinates are given with respect to the reference frame used in the figure and will define later interlayer distances. (b) The five Ag0 atoms also sit on the mirror plane (z_0=3.88 Å). (c) Two Cu1 atoms sitting on the five-fold rotation axis symmetrically located above and below the mirror plane (z_1=5.17 Å and z_{-1}=2.59 Å). Notice that the Cu0 pentagon fits in the Ag0 pentagon. (d) Ten Ag2 atoms form two pentagons symmetrically located above and below the mirror plane (z_2=5.31 Å and z_{-2}=2.44 Å). (e) Ten Ag3 form two pentagons symmetrically located above and below the mirror plane (z_3=6.24 Å and z_{-3}=1.52 Å). (f) The two Ag4 atoms sit on the five-fold rotation axis symmetrically located above and below the mirror plane (z_4=7.76 Å and z_{-4}=0 Å).

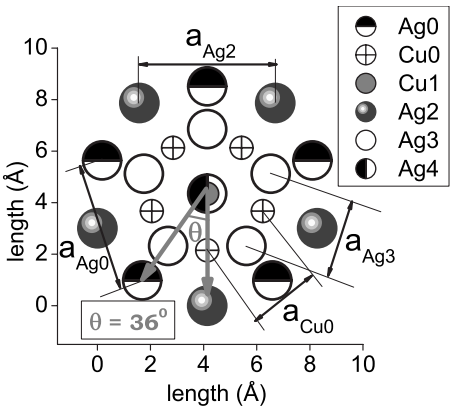

FIG. 2. *Top view* of $Ag_{27}Cu_7$ nanoalloy, perpendicular to the mirror plane. The side length of each pentagon is a_{Mn} (see text).

TABLE I. This table contains six sets of two-column *subtables* showing the distance from each type of atom in the nanoalloy to all its neighbors. In the right column of each subtable appears the type of neighbor that is being referred to and the number of such equivalent atoms at the same distance is shown in parentheses. Notice here that equivalent atoms are not considered if they do not belong to the same layer.

Cu0		Ag0		Cu1		Ag2		Ag3		Ag4	
Type (NN)	d (Å)	Type (NN)	d (Å)	Type (NN)	d (Å)	Type (NN)	d (Å)	Type (NN)	d (Å)	Type (NN)	d (Å)
$Cu1^{(1)}$	2.548	$Cu0^{(2)}$	2.715	$Cu0^{(5)}$	2.548	$Cu0^{(1)}$	2.587	$Cu1^{(1)}$	2.726	$Cu1^{(1)}$	2.590
$Cu\text{-}1^{(1)}$	2.548	$Ag3^{(1)}$	2.882	$Cu\text{-}1^{(1)}$	2.576	$Ag\text{-}2^{(1)}$	2.867	$Cu0^{(2)}$	2.786	$Ag3^{(5)}$	2.932
$Cu0^{(2)}$	2.584	$Ag\text{-}3^{(1)}$	2.882	$Ag4^{(1)}$	2.590	$Ag3^{(2)}$	2.902	$Ag0^{(1)}$	2.882	$Cu0^{(5)}$	4.457
$Ag2^{(1)}$	2.587	$Ag2^{(2)}$	3.002	$Ag3^{(5)}$	2.726	$Ag0^{(2)}$	3.002	$Ag2^{(2)}$	2.902	$Ag2^{(5)}$	4.991
$Ag\text{-}2^{(1)}$	2.587	$Ag\text{-}2^{(2)}$	3.002	$Ag2^{(5)}$	4.354	$Cu1^{(1)}$	4.354	$Ag4^{(1)}$	2.932	$Cu\text{-}1^{(1)}$	5.166
$Ag0^{(2)}$	2.715	$Cu1^{(1)}$	4.360	$Ag0^{(5)}$	4.360	$Cu0^{(2)}$	4.462	$Ag3^{(2)}$	2.948	$Ag0^{(5)}$	5.691
$Ag\text{-}3^{(2)}$	2.786	$Cu\text{-}1^{(1)}$	4.360	$Ag\text{-}3^{(5)}$	4.425	$Ag\text{-}3^{(2)}$	4.684	$Cu\text{-}1^{(1)}$	4.425	$Ag\text{-}3^{(5)}$	6.721
$Ag3^{(2)}$	2.786	$Ag3^{(2)}$	4.769	$Ag\text{-}2^{(5)}$	5.132	$Ag4^{(1)}$	4.991	$Cu0^{(2)}$	4.482	$Ag\text{-}2^{(5)}$	6.866
$Cu0^{(2)}$	4.181	$Ag\text{-}3^{(2)}$	4.769	$Ag\text{-}4^{(1)}$	5.166	$Ag2^{(2)}$	5.115	$Ag\text{-}2^{(2)}$	4.684	$Ag4^{(1)}$	7.756
$Ag4^{(1)}$	4.457	$Ag0^{(2)}$	4.897			$Cu\text{-}1^{(1)}$	5.132	$Ag\text{-}3^{(1)}$	4.716		
$Ag\text{-}4^{(1)}$	4.457	$Cu0^{(2)}$	5.277			$Ag3^{(2)}$	5.729	$Ag0^{(2)}$	4.769		
$Ag2^{(2)}$	4.462	$Ag4^{(1)}$	5.691			$Ag\text{-}2^{(2)}$	5.864	$Ag3^{(2)}$	4.770		
$Ag\text{-}2^{(2)}$	4.462	$Ag\text{-}4^{(1)}$	5.691			$Cu0^{(2)}$	6.426	$Cu0^{(1)}$	5.263		
$Ag3^{(2)}$	4.482	$Cu0^{(1)}$	6.364			$Ag\text{-}3^{(2)}$	6.807	$Ag\text{-}3^{(2)}$	5.561		
$Ag\text{-}3^{(2)}$	4.482	$Ag3^{(2)}$	6.790			$Ag\text{-}4^{(1)}$	6.866	$Ag2^{(2)}$	5.729		
$Ag3^{(1)}$	5.263	$Ag\text{-}3^{(2)}$	6.790			$Ag3^{(1)}$	6.921	$Ag\text{-}3^{(2)}$	6.707		
$Ag\text{-}3^{(1)}$	5.263	$Ag2^{(2)}$	7.039			$Ag0^{(2)}$	7.039	$Ag\text{-}4^{(1)}$	6.721		
$Ag0^{(2)}$	5.277	$Ag\text{-}2^{(2)}$	7.039			$Ag\text{-}3^{(1)}$	7.837	$Ag0^{(2)}$	6.790		
$Ag0^{(1)}$	6.364	$Ag0^{(2)}$	7.923			$Ag2^{(2)}$	8.277	$Ag\text{-}2^{(2)}$	6.807		
$Ag2^{(2)}$	6.426	$Ag2^{(1)}$	8.637			$Ag0^{(1)}$	8.637	$Ag2^{(1)}$	6.921		
$Ag\text{-}2^{(2)}$	6.426	$Ag\text{-}2^{(1)}$	8.637			$Ag\text{-}2^{(2)}$	8.759	$Ag\text{-}2^{(1)}$	7.837		

2. *Neighbor distances in* $Ag_{27}Cu_7$*: A comparison with bulk Ag and bulk Cu values*

Despite the perfect D_{5h} symmetry of the cluster, Table I shows an intricate hierarchy of bond lengths in the optimized structure. For example, Ag3 atoms have nine neighbors spread in a range from 2.726 to 2.948 Å, all within a separation equal to the bond length of Ag bulk. Figures 3(a) and 3(b) show a comparison between the bond coordination of atoms in the $Ag_{27}Cu_7$ nanoalloy and that of atoms in bulk Ag and bulk Cu. Notice from Table I that the local coordination of Cu atoms in $Ag_{27}Cu_7$ seems, in fact, not dramatically different from that in bulk Cu regarding the number of first and second nearest neighbors (NNs). The Cu0 atoms, for example, have 12 neighbors within a distance from 2.548 to 2.786 Å, and another 12 between 4.181 and 4.482 Å. Silver atoms, on the other hand, find themselves in unusual atomic environments: at a distance of 3 Å (bulk Ag nearest neighbor distance) Ag2 and Ag4 atoms have barely acquired six neighbors, while Ag3 and Ag0 atoms get nine and eight NNs, respectively. Between 4.2 and 4.5 Å, at which bulk Ag atoms already have 18 NNs, Ag0, Ag3, and Ag4 atoms have acquired at most 11 neighbors, while Ag2 atoms have only seven NNs, finding themselves as the most undercoordinated atoms of the cluster. Most importantly, we notice that the NN bond lengths between Cu atoms contract by as much as 2% with respect to the value in bulk (2.599 Å). Such a contraction may be expected for Cu atoms in low coordination environments, such as on the surface layer of Cu(100) [inward contraction of around 3% (Ref. 23)], and not in $Ag_{27}Cu_7$ because of their high coordination (12) as in bulk Cu. Interestingly, for the shell Ag atoms, which have a much lower local coordination than the core Cu atoms, the Ag-Ag NN bond lengths are at most ~2.6% shorter than those in bulk Ag (2.943 Å). If coordination

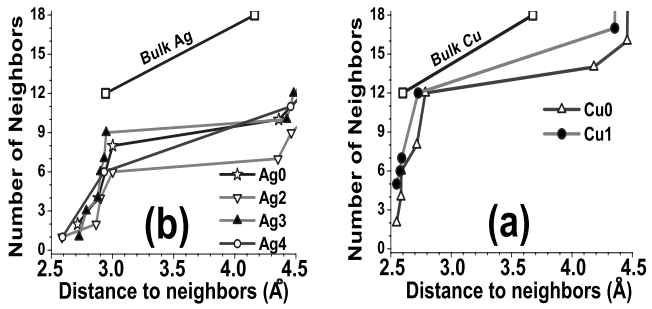

FIG. 3. (a) Bond coordination for Cu atoms of $Ag_{27}Cu_7$ as compared with Cu bulk. (b) Bond coordination for Ag atoms of $Ag_{27}Cu_7$ as compared with Ag bulk.

alone were a measure, one might have expected the most undercoordinated Ag atoms, Ag2 and Ag4, to undergo a larger contraction, as found on Ag surfaces.[23] Instead, in $Ag_{27}Cu_7$, Ag2 and Ag4 form short bonds of about 2.59 Å with their neighboring Cu atoms, as seen from Table I. These bond lengths are, in fact, very close to the smallest Cu-Cu bond lengths (2.55 Å) and considerably smaller than the smallest Ag-Ag bond lengths (2.87 Å). Indeed, it follows from Table I that in $Ag_{27}Cu_7$, the first NN of every Ag atom is a Cu atom, pointing to the reality that finite-sized structures of these elements may not follow straightforwardly the behavior of infinite and/or semi-infinite systems and the relationship between bond coordination number and bond stiffening might be subtler in nanoalloys. Two conclusions may, nevertheless, be drawn from the above discussion (1) the fact that Cu-Cu bond lengths in $Ag_{27}Cu_7$ contract almost as much as Ag-Ag bond lengths suggests that Cu atoms are more sensitive than Ag atoms to either low coordination, local geometry, or chemical environment; (2) the low coordination of the Ag atoms appears to be significantly compensated by the formation of short bond lengths with Cu atoms. To discriminate between the above mentioned effects of local coordination, geometry, and environment, the conclusions about bond lengths in the $Ag_{27}Cu_7$ nanoalloy need to be put on firmer grounds through examinations of the details of the electronic structure and the charge density distribution, and their implications for nanoalloy stability. We will turn to this in Secs. III A 4 and III B. However, before we do that, it is interesting to examine the structural stability of related bulk alloys, Ag_3Cu and Cu_3Ag, for which some information already exists and, hence, can serve as reference points. The relationship between the compositions of $Ag_{27}Cu_7$ and Ag_3Cu is obvious. The other alloy is chosen to establish whether the preponderance of Cu and/or its effect on bond lengths is a key for understanding the structural stability of these alloys.

3. *Structure, phonons, and heat of formation of* Cu_3Ag *and* Ag_3Cu *bulk alloys*

In considerations of structural stability of bulk alloys, it is essential that the heat of formation be negative and that the phonon spectrum be well defined. Ag-Cu alloys, unlike Au-Cu and Au-Ag alloys, are known for their tendency to segregate and have a miscibility gap beyond the eutectic temperature of the material.[20–22] Earlier calculations[20–22] have shown that Ag-Cu alloys possess a positive heat of formation regardless of the chosen ratio of Ag to Cu.[20,21] In particular, the heat of formation per atom was found to be about 70 meV for Ag_3Cu (60 meV, in this work) and 80 meV for Cu_3Ag (64 meV, in this work), pointing to the structural instability of these Ag-Cu bulk alloys.[21]

It has, however, been pointed out that even with a positive heat of formation, the presence of a well-defined phonon spectrum may serve as an indicator of alloy stability under special formation conditions, for example, using nonequilibrium techniques.[39–42] Indeed, among a variety of immiscible noble-transition metal alloys, some—particularly those that mix fcc and hcp metals—have shown mutual solid solubility.[43] Kong *et al.*[39] calculated the phonon spectra of several structures of the equilibrium immiscible Ag_xRu_y bulk alloys, for $x/y=1/3$ and 3, to find that only the $L1_2$ and $D0_{19}$ phases of Ru_3Ag may be stable. In Ref. 39, phonon-stable or -unstable structures were associated with the presence of relatively high charge density bridging NN atoms of the same or different element. We will discuss charge density implications later in Sec. III B 2. For the present discussion, we note that, regardless of the structure of the stable phases, the phonon-stable Ag-Ru alloys are all Ru-rich and have a smaller lattice parameter than the corresponding Ag-rich structures, owing to the fact that typical bond lengths in bulk Ru are smaller than those in bulk Ag. Moreover, Kong *et al.* were able to remove the phonon instabilities, when present, by artificially increasing the external pressure, i.e., by simply reducing the equilibrium lattice parameter.

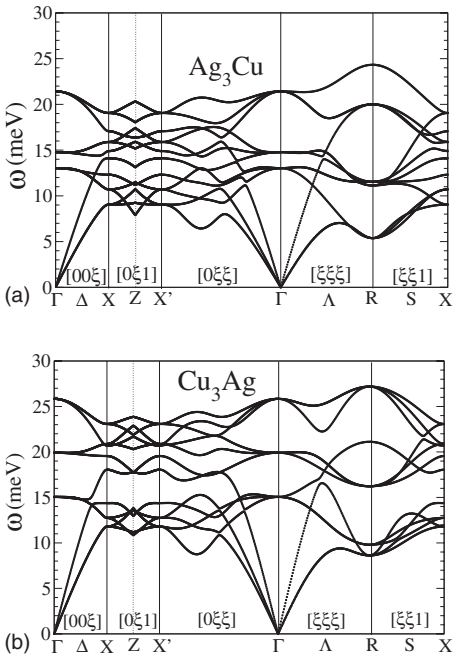

FIG. 4. Calculated phonon spectra of the hypothetical $L1_2$ phase of (a) Ag_3Cu and (b) Cu_3Ag bulk alloys.

In the above spirit, we now turn to the calculation of the structure and the lattice dynamics of Ag_3Cu and Cu_3Ag bulk alloys by using DFT and DFPT methods. We find the bond length of Ag_3Cu to be 2.87 Å and that of Cu_3Ag to be 2.70 Å. For reference, note that our calculated bond lengths for bulk Cu and Ag are 2.59 and 2.94 Å, respectively. Note also that the shortest Ag-Cu bond lengths in $Ag_{27}Cu_7$ are around 2.6 Å. The bond lengths in bulk alloys Ag_3Cu and Cu_3Ag are thus larger than the shortest Ag-Cu bond length in the nanoalloy and that in bulk Cu and may imply the lack of overlap of the *d* orbitals for its Ag-Cu and Cu-Cu bonds (as we shall see), pointing to the structural instability of these bulk alloys. Our calculated phonon dispersion curves (Fig. 4) of Ag_3Cu and Cu_3Ag, showing the absence of unstable modes, however, suggest that these alloys may be stable and obtainable by nonequilibrium techniques.[39]

Furthermore, phonon dispersion curves are a measure of the contribution of the vibrational entropy to the free energy of a given system.[44] The vibrational entropy integrates the vibrational DOS weighted by a factor that falls off as the

frequency of phonons increases. Thus, vibrational entropy plays a larger role in the minimization of the free energy for systems whose (well-defined) phonon dispersion curves display notable contributions and shifts of the density of states toward the lower frequency range.[22] For example, bulk Cu_3Au ($L1_2$) has a larger vibrational entropy than either bulk Au or Cu.[45] Our calculated phonon dispersion for bulk Ag_3Cu [see Fig. 4(a)] is softer than that of bulk alloy Cu_3Ag [Fig. 4(b)], bulk Ag,[46] and bulk Cu,[46] indicating that the vibrational entropy of Ag_3Cu is larger than those of bulk Ag and Cu. Regardless, the vibrational entropic contribution to the reduction in the free energy is small[22] (typically less than 5 meV at room temperature) as compared to the positive heat of formation (~60 meV) found for this bulk alloy. Instead, the presence of a stiffer vibrational DOS of Cu_3Ag, as compared to that of Ag_3Cu, reflects stronger bonds in the former, which may provide stability if created by the techniques mentioned above.[39–42]

4. Formation energy of $Ag_{27}Cu_7$

In Ref. 1, the thermodynamic stability of a given nanoalloy is evaluated via considerations of its melting temperature and its relative energetic stability is established through a comparison of the heats of formation, Δ, adapted to binary clusters as follows:

$$\Delta(\mathrm{Ag}_{N_1}\mathrm{Cu}_{N_2}) = \frac{E(\mathrm{Ag}_{N_1}\mathrm{Cu}_{N_2}) - N_1E(\mathrm{Ag}_{bulk}) - N_2E(\mathrm{Cu}_{bulk})}{N^{2/3}}, \tag{1}$$

where $N=N_1+N_2$, $E(\mathrm{Ag}_{N_1}\mathrm{Cu}_{N_2})$ is the total energy of the nanocluster, and $E(\mathrm{Cu}_{bulk})$ and $E(\mathrm{Ag}_{bulk})$ are the total energies of one Cu and one Ag atom, respectively, in the bulk phase. Remarkably, although clusters with increasing binding energies per atom do not necessarily have higher melting temperatures,[47] $Ag_{27}Cu_7$ came out with both the highest melting point and the least heat of formation. In terms of stability and minimum-energy structures, however, it is important to know also the output given by the average formation energy, which measures the dissociation or *cohesive* energy of the nanoalloy, and to analyze the meaning, implications, and scope of these two energetic considerations. Thus, to estimate the average strength of the bonds, we calculate the so-called average formation energy per atom, E_{form}, which is defined as

$$E_{form}(\mathrm{Ag}_{N_1}\mathrm{Cu}_{N_2}) = \frac{E(\mathrm{Ag}_{N_1}\mathrm{Cu}_{N_2}) - N_1E(\mathrm{Ag}_{free}) - N_2E(\mathrm{Cu}_{free})}{N}, \tag{2}$$

where $E(\mathrm{Cu}_{free})$ and $E(\mathrm{Ag}_{free})$ are the energies of isolated Cu and Ag atoms, respectively. We find $E_{form}(Ag_{27}Cu_7)$ to be 2.17 eV. Since no experimental data on this particular binary nanocluster exist, we turn to the formation energy of related systems for comparison. For example, our calculated cohesive energies of bulk Ag, Ag_3Cu, Cu_3Ag, and Cu are 2.51, 2.66, 3.06, and 3.34 eV, respectively, implying that $E_{form}(Ag_{27}Cu_7)$ is smaller than all these bulk values. Note that the higher cohesive energy of bulk Ag_3Cu as compared to that of bulk Ag signals a stronger Ag-Cu bond than the usual Ag-Ag one. In fact, from the results presented in Ref. 1, one finds that the average formation energy per atom of the 34-atom family decreases monotonically from ~2.6 to ~2.0 eV as the Ag content increases from 0 to 34. Considerations of formation energy alone would thus imply that in this family of nanoalloys, the Cu-Cu and Cu-Ag bonds are stronger than the Ag-Ag bonds and that $Ag_{27}Cu_7$ is not the most stable structure. It is thus surprising that a related quantity, i.e., the heat of formation [defined as in Eq. (2), but substituting $E(\mathrm{Cu}_{free})$ and $E(\mathrm{Ag}_{free})$ by the cohesive energies of Cu and Ag, respectively], plotted as function of the Ag/Cu ratio in Ref. 1, shows a minimum at this intermediate composition ($Ag_{27}Cu_7$)—a result that stands in contrast to that found in Ag-Cu bulk alloys.[20–22] Nevertheless, we find that the heat of formation of $Ag_{27}Cu_7$ is nine times larger than that of bulk Ag_3Cu, but this suggestion of instability might be misleading since the heat of formation not only measures the strength of the bonds but also weighs the energetic cost (gain) of breaking (forming) single element bulk bonds to form (from breaking) binary bonds. In reality, the formation of intricately tailored structures as $Ag_{27}Cu_7$ is not expected to occur simply by melting the parent compounds. Thus, measures like heat of formation have to be supplemented by others such as the dynamical stability of the alloy as displayed by its vibrational modes. The heat of formation is perhaps more of an indicator of the lifetime of the nanoalloy, say, against clustering and the eventual formation of segregated metallic bulk Cu and Ag, if one ignores the energy barriers needed to actually break all of the bonds in the nanoalloy.

On the experimental side, in addition, we note that the pure clusters Ag_7^- (Ref. 47) and Ag_{19}^+ (Ref. 48) were found to have dissociation energies of 2.73 and 2.88 eV, which are very close to the experimentally observed cohesive energy of bulk Ag (2.94 eV). The formation of pure cluster structures, such as Ag_7^- and Ag_{19}^+, may thus be seen to be energetically more favorable than the nanoalloys. Perhaps, the possible disintegration of $Ag_{27}Cu_7$ into pure-element clusters may be argued against on the basis of the strength of the Ag-Cu bond. To estimate the strength of the bonds in the 34-atom nanoalloys and understand what distinguishes $Ag_{27}Cu_7$ in its family of nanoalloys, we turn to Fig. 2 of Ref. 1. Rossi *et al.* showed that as the amount of Cu increases up to ~20% (starting from Ag_{34}), the heat of formation is reduced or kept constant, implying that small amounts of Cu atoms immersed among Ag atoms (in the nanoalloys $Ag_{34-n}Cu_n$ as n decreases from 7 to 1) create Cu-Ag and Cu-Cu bonds that are stronger than those in bulk Cu and are able not only to counterbalance the cost of the cohesive energy of the newly added Cu atom but also to increasingly stabilize the nanoalloy. Figure 2 of Ref. 1 shows also that if the content of Cu increases beyond seven atoms, the heat of formation increases again, with the implication that the strength of the bonds is not able to compensate for the bulk Cu cohesive energy for an additional atom. In conclusion, $Ag_{27}Cu_7$ possesses the composition and geometry that maximize the number of Cu-Cu and Cu-Ag bonds with the minimum number of Cu atoms.

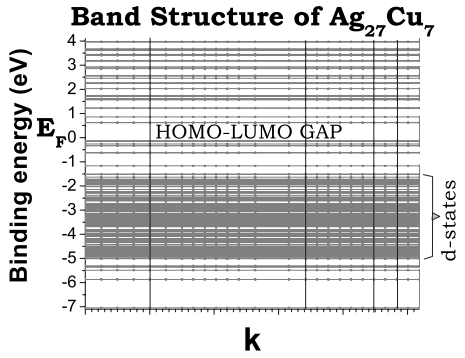

FIG. 5. Band structure of $Ag_{27}Cu_7$ showing that the bands do not depend on $\boldsymbol{k}$ (see Ref. 35) and that the d states are concentrated between −5.0 and −1.5 eV below the Fermi level (see text).

The structural stability considerations presented above are derived entirely from the energetics of $Ag_{27}Cu_7$. The contributions of vibrational entropy could be important[18] and may lead to a minimum of the free energy (as a function of the Ag/Cu ratio), which is different from that in the plot of Rossi *et al.* They, however, argue against such a possibility.[1] Very recent calculations[49] based on many-body interaction potentials also confirm that vibrational entropic contributions are small for this set of 34-atom nanoalloys. Calculations of the phonon frequencies of these nanoalloys from first principles, as presented in Sec. III A 3 for the Ll_2 bulk alloys, are still desirable, as such a study could serve as an indicator of stable compositions. However, the resulting contributions of the vibrational entropy to the free energy are expected to be small and should not change the conclusions drawn here. Configurational entropy may, in general, also play a role in determining the stable configurations of these nanoalloys, but it is not expected to be important for $Ag_{27}Cu_7$ because of the lack of degenerate isomers.[50]

B. Electronic structure and charge density distribution

1. *Electronic density of states of* $Ag_{27}Cu_7$ *nanoalloy and* Ll_2 Ag-Cu *alloys*

In our calculations, the $Ag_{27}Cu_7$ nanoalloy has 374 valence electrons occupying 187 discrete, flat, and double degenerated bands, as shown in Fig. 5. As we can see, the discrete d states are densely concentrated between −5.0 and −1.5 eV below the Fermi level. Such an ideal behavior of the DOS may not be observed in experiments.[19] One of the reasons is that the Jahn–Teller deformation, which lifts the degeneracy of the levels, smears out the ideal DOS, and may also lead to the opening of gaps, is not included in the present approach.[19] The second reason is that the actual atomic positions occurring in a cluster due to deviations from the ideal structure further modifies the DOS.[19] For example, Ref. 19 shows that the photoelectron spectrum of Cu_{34}^- (among others smaller and larger) is significantly smoother than 187 sharp peaks that one may expect, though it does display smooth dips. To obtain the electronic DOS of bulk Cu_3Ag and Ag_3Cu alloys and $Ag_{27}Cu_7$ nanoalloy from *ab initio* electronic structure calculations, the states are thus broadened by using Gaussian functions of width 0.14 eV.

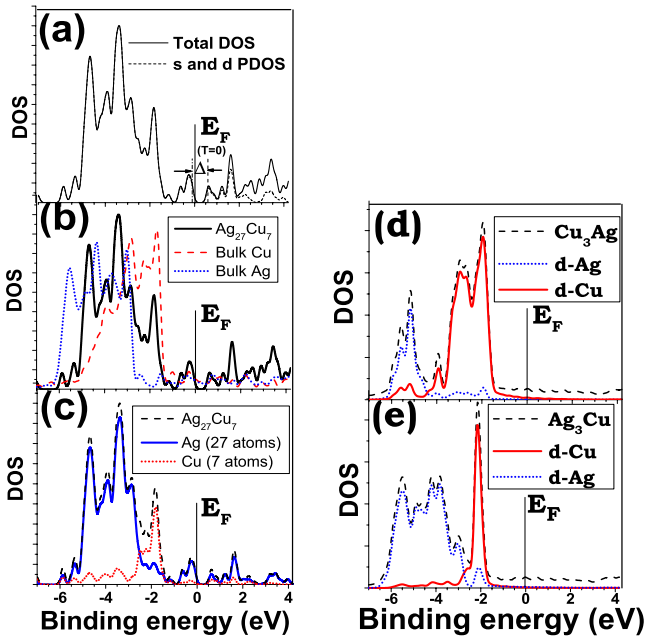

FIG. 6. (Color online) (a) Total and projected electronic DOS of $Ag_{27}Cu_7$. The latter corresponds to the contribution of s and d atomic states between −7 and 4.2 eV from the Fermi level, E_F, which is set equal to 0. The s contribution is negligible up to E_F. The HOMO-LUMO gap in the ground state (Δ=0.77 eV) is highlighted in red. (b) Comparison between the total DOS of $Ag_{27}Cu_7$ and that of Ag and Cu bulk. (c) Contribution from the core (Cu) and shell (Ag) atoms to the projected DOS of $Ag_{27}Cu_7$. (d) DOS of Cu_3Ag showing the d contribution from each species to the total DOS of the alloy in the $L1_2$ phase. (e) DOS of Ag_3Cu showing the d contribution from each species and the total DOS of the alloy in the $L1_2$ phase.

Our resulting DOS of $Ag_{27}Cu_7$ is shown in Figs. 6(a)–6(c), while that of the bulk alloys is presented in Figs. 6(d) and 6(e). First of all, the HOMO-LUMO gap [Δ in Fig. 6(a)] of $Ag_{27}Cu_7$ is found to be 0.77 eV in the ground state, which is only slightly smaller than that reported by Rossi *et al.* (0.82 eV).[1] As expected, the s states have negligible contributions and the displayed structures have mostly a d character between −5.3 and −1.5 eV. Figure 6(b) shows that the centroid ($\frac{\int Ef(E)dE}{\int f(E)dE}$) of the nanoalloy valence band redshifts by ~1 eV as compared to bulk Ag and blueshifts by ~0.5 eV with respect to bulk Cu. Figure 6(c) shows that even though the amount of Cu in the $Ag_{27}Cu_7$ nanoalloy is about four times less than that of Ag, it contributes to blueshift the valence band. As shown in Figs. 6(c)–6(e) and in Refs. 17 and 51, the role of Cu is, in general, to enhance the DOS at the top of the valence band and to blueshift the centroid, while the effect of Ag is the opposite. Similar results have been reported for Au-Pd nanoclusters,[52] in which the increasing content of Au on Pd clusters reduces the density of states at the Fermi level. Figures 6(b) and 6(c) show, in addition, that the d-band of the nanoalloy is as broad as that of either pure bulk constituents—a point worth noticing since atoms in a low-coordinated environment generally exhibit a valence band narrowing.[53] Pure Ag clusters and Cu_3Au surfaces,[51,53]

for example, have shown this effect. The hybridization of Ag and Cu states in $Ag_{27}Cu_7$ thus compensates for the *d*-band narrowing that each atom undergoes.

In general, the features in the electronic DOS that discriminate stable alloy phases are not yet fully understood. Although it is well accepted[20] that the dip in the DOS at the Fermi level is related to the stability of a particular alloy phase, there is no obvious correlation between the two since stable and ordered Cu-Au alloys present a dip in the DOS, while Au-Ag alloys do not.[20] In the former, the dip in the DOS changes position, width and depth with composition, and structure, and has been found to be related to the electronic specific heat.[17] Kokko *et al.*[17] noticed also that the dip is considerably lessened in the layered (tetragonal $L1_0$) CuAuI phase (which reduces the Au-Cu bond) with respect to Cu_3Au and Au_3Cu. Also, based on their electronic specific heat calculations, they infer that the dip is even smoother in the disordered phases. In this work, we find that the nanoalloy $Ag_{27}Cu_7$ displays a less pronounced dip (deepest at ~ −2.25 eV) in the *d*-band region (between ~−5.3 and ~ −1.5 eV), where Cu and Ag states hybridize, than those displayed by Ll_2 Cu_3Ag and Ag_3Cu alloys [deepest at ~−3.6 and ~−2.5 eV, respectively; cf. Figs. 6(a), 6(d), and 6(e)], which are similar to, but broader than, those found in stable Cu-Au alloys.[17] Yet, from considerations of the heat of formation, the Ag-Cu alloys are marked as being immiscible. Furthermore, we find that the DOS of the Ag atoms [Figs. 6(b) and 6(c)] in $Ag_{27}Cu_7$ resembles to some extent that of bulk Ag, despite being highly undercoordinated, while that of the fully coordinated Cu atoms is strikingly different from that of bulk Cu, presumably since half of its neighbors are Ag atoms.

In order to understand the correlation between the Ag/Cu content ratio, the consequent decrease or increase in the bond lengths, and the structure of the electronic DOS, we turn to an examination of the changes experienced by the DOS of individual Ag and Cu atoms in a set of environments (some natural, some artificial): $Ag_{27}Cu_7$ nanoalloy, freestanding Ag and Cu monolayers, bulk Ag-Cu alloys, and bulk Ag and Cu (Figs. 7–9). For the bulk systems, we consider also the effect on the DOS (Fig. 8) of expanding and contracting the lattice constant from the equilibrium value found in our DFT calculations. The DOS of Ag and Cu atoms in Figs. 7–9 allow for a comparison on a *one-to-one* basis and not as percentile contributions as presented in Fig. 6.

From Figs. 7(a) and 7(b), we note that a decrease in the content of Ag (and thus the lattice parameter) gives rise to a sharp peak at intermediate energies, while the bottom of the *d*-band remains almost unchanged and states from the top of the bulk Ag band [Fig. 7(e)] retract to lower energies. A few states, however, appear between −1.5 and −2.5 eV, above the range of the DOS of bulk Ag, and hybridize with Cu states. As we shall see, the appearance of these higher energy states is related purely to the presence of Cu, whereas the depletion of the top of the Ag *d*-band results from both the presence of Cu and from the enhanced overlap of Ag-Ag orbitals as a result of the decrease in the Ag-Ag bond length.

To isolate the effect of the bond length, we turn to the DOS in Fig. 8 for Ag and Cu atoms in bulk environments with bond lengths different from the equilibrium values. In

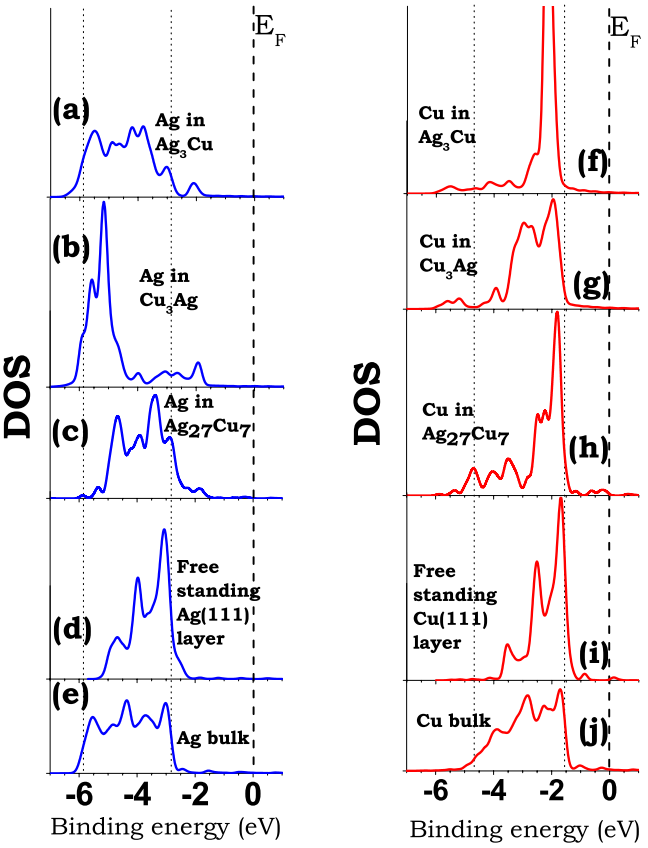

FIG. 7. (Color online) Electronic DOS (*d*-band) of Cu and Ag atoms situated in various environments and bond length (l); (a) Ag atoms in Ag_3Cu (l=2.87 Å), (b) Ag atoms in Cu_3Ag (l=2.70 Å), (c) Ag atoms in $Ag_{27}Cu_7$, (d) Ag atoms in Å freestanding Ag(111) monolayer (l=2.94 Å), (e) Ag atoms in bulk (l=2.94 Å), (f) Cu atoms in Ag_3Cu (l=2.87 Å), (g) Cu atoms in Cu_3Ag (l=2.70 Å), (h) Cu atoms in $Ag_{27}Cu_7$, (i) Cu atoms in Å free standing Cu(111) monolayer (l=2.59 Å), and (j) Cu atoms in bulk (l=2.59 Å).

order to maintain a reference point, we have taken the lattice constant of expanded Ag_3Cu and Cu_3Ag to be that of bulk Ag, corresponding to an expansion of 2.4% in the former and 8.9% in the latter. Similarly, to infer the effect of lattice contraction, we have used the lattice constant of bulk Cu for Ag_3Cu (contraction of 9.8%) and the bond length of Cu0-Cu1 for Cu_3Ag (contraction of 5.5%). By comparing Figs. 7(e) and 8(f), we find that the contraction of Ag-Ag bonds pushes the bottom of the Ag *d*-band to lower energies and depletes the top of the band, while a comparison of Fig. 7(a) with Fig. 8(b) and Fig. 7(b) with Fig. 8(d) indicates that the contraction of Ag-Cu bonds also pushes the bottom of the Ag *d*-band to lower energies and significantly lessens the highest features of the DOS of the Ag *d*-band in bulk alloys. We also conclude from Figs. 8(b) and 8(d), and Fig. 7(e), 7(a), and 7(b), that the presence of Cu is responsible for the appearance of Ag states above the top of the bulk Ag band, hence improving the overlap with the Cu *d*-band. On the other hand, as seen from Figs. 7(e) and 8(e), the expansion of Ag-Ag bonds depletes the bottom of the DOS and slightly enhances the DOS at the top. Similarly, the expansion of the Ag-Cu bond in the bulk alloys depletes the bottom of the

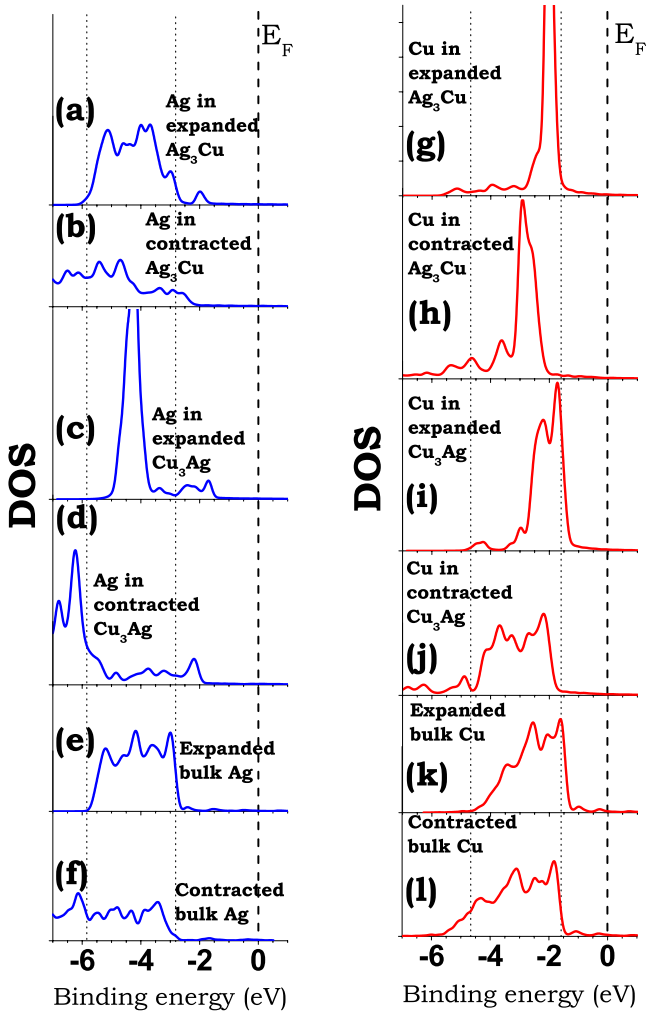

FIG. 8. (Color online) Electronic DOS (d-band) of Cu and Ag atoms in pure bulk and $L1_2$ bulk Ag-Cu alloys with expanded on contracted l: (a) Ag atoms in 2.4% expanded Ag_3Cu with $l=l_{Ag_{bulk}}=2.94$ Å, (b) Ag atoms in 9.8% contracted Ag_3Cu with $l=l_{Cu_{bulk}}=2.59$ Å, (c) Ag atoms in 8.9% expanded Cu_3Ag with $l=l_{Ag_{bulk}}$, (d) Ag atoms in 5.5% contracted Cu_3Ag with $l=d(\mathrm{Cu0}-\mathrm{Cu1})=2.55$ Å, (e) Ag atoms in 8.0% expanded bulk Ag; (f) Ag atoms in 11.9% contracted bulk Ag with $l=l_{Cu_{bulk}}$, (g) Cu in 2.4% expanded Ag_3Cu, (h) Cu in 9.8% contracted Ag_3Cu, (i) Cu in 8.9% expanded Cu_3Ag, (j) Cu in 5.5% contracted Cu_3Ag, (k) Cu in 8.0% expanded bulk Cu, and (l) Cu in 1.6% contracted bulk Cu.

DOS and enhances the highest peaks of the DOS [cf. Fig. 7(a) with Fig. 8(a) and Fig. 7(b) with Fig. 8(c)]. Atomic low coordination and expansion of the bond length cause the same effects on the DOS of Ag, though these are augmented in the former situation. Such was found to be the case of a freestanding (111) monolayer [Fig. 7(d)], in which the six coordination of Ag atoms causes a strong depletion of the bottom and an enhancement at the top of the d-band.

From the above discussion, we conclude that the low coordination of Ag atoms in the $Ag_{27}Cu_7$ nanoalloy can, indeed, account for the depletion of the bottom of the d-band [Fig. 7(c)]. On the other hand, the reduction in the DOS at the top of the d-band of Ag0 [Fig. 9(a)], Ag3 [Fig. 9(c)], and Ag4 [Fig. 9(d)] atoms suggests that the presence of Cu at

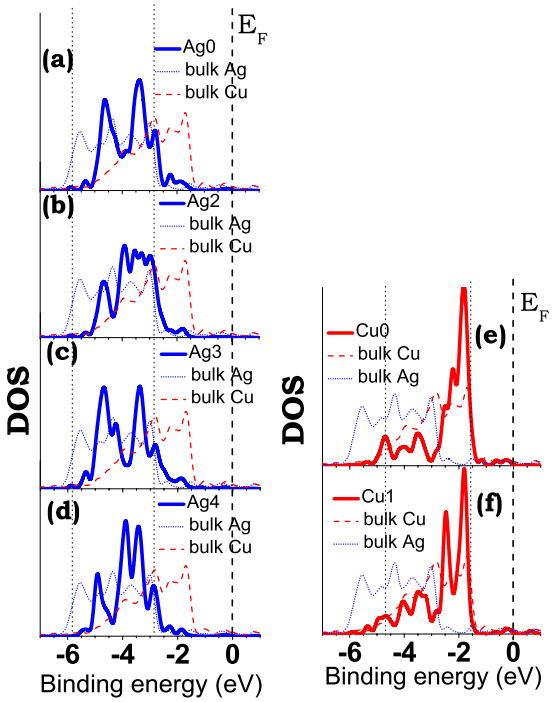

FIG. 9. (Color online) The PDOS of the six nonequivalent types of atoms in the $Ag_{27}Cu_7$ nanoalloy is compared with the DOS of pure bulk Cu (dashed lines) and Ag (dotted lines). E_F is shifted to 0 for all of them: (a) Ag0, (b) Ag2, (c) Ag3, (d) Ag4, (e) Cu0, and (f) Cu1.

such short distances outweighs the effect of their low coordination and the DOS at the top of the Ag d-band is not enhanced. The DOS of Ag2 is slightly more complex. As mentioned in Sec. III A 2, Ag2 is the most undercoordinated atom of the cluster (see Fig. 3). Consistently, it has the least number of states below −4.5 eV and the highest DOS above ~−2.8 eV, implying that low coordination effects on the DOS of Ag2 are not completely washed out through the short bond with Cu0, each of which is incidentally shared by two Ag2 atoms. At the same time, as seen in bulk alloys, the hybridization of Cu and Ag states is improved by setting off the occupation of states above the top of the d-band of bulk Ag [see Fig. 7(c) and Figs. 9(a)–9(d)].

We now turn to the issue of the DOS of Cu atoms in the $Ag_{27}Cu_7$ nanoalloy, which differs prominently from that of bulk Cu. We consider three different aspects that may influence their electronic structure: the conspicuously disparate overall geometry, the presence of Ag, and the existence of bond lengths longer than that of bulk Cu. To understand each one of these, we first note that if Cu-Ag bonds are longer than that of bulk Cu, then the bottom of the d-band of Cu is strongly depleted and an increasingly sharper peak at the top is created, which slightly shifts toward higher energies [cf. Fig. 7(f) with Fig. 8(g) and Fig. 7(g) with Fig. 8(i)]. As already noted for the Ag atoms, the effect of expanding Cu-Cu bonds is similar to that of Cu atoms in a low-coordinated environment [cf. Figs. 8(k) and 7(i) with Fig. 7(j)], that is, the bottom of the Cu d-band [states below ~3.5 and ~4.0 eV in Figs. 7(i) and 8(k), respectively] is entirely extinguished. Interestingly, the d-band of the free monolayer

is sharply localized at the top edge, resembling those of Cu0 [Fig. 9(e)] and Cu1 [Fig. 9(f)] atoms, notwithstanding their full coordination in $Ag_{27}Cu_7$. Contracting Ag-Cu bonds in bulk alloys reduces the DOS at the top, which is pushed to lower energies, and enhances the bottom of the *d*-band, thus improving the Ag-Cu hybridization, as seen by comparing Fig. 7(f) with Fig. 8(h) and Fig. 7(g) with Fig. 8(j). Similar features are found by contracting the Cu-Cu bond in bulk Cu [cf. Figs. 7(j) and 8(l)]. More importantly, note in Fig. 8(j) that even when Cu-Cu and Cu-Ag bonds in contracted bulk Cu_3Ag are shorter than that of bulk Cu, the region from ~4.0 to ~5.0 eV is, nevertheless, strongly quenched, suggesting that the presence of Ag also strongly depletes most of the bottom of the *d*-band of Cu atoms (something similar occurs in Au-Cu, see Ref. 17). Observe also that the presence of Ag introduces states below the bottom of the DOS of bulk Cu [Figs. 7(f)–7(h) and Figs. 8(g)–8(j)], which hybridize with Ag.

From the above discussion, we conclude first that the sharp peak [Fig. 7(h)] at the top of the DOS of Cu atoms in the $Ag_{27}Cu_7$ nanoalloy, characteristic of low coordination [Fig. 7(i)], can only be accounted for by the relatively long distances (~2.7–2.8 Å) between Cu atoms and half of their *nearest neighbors*—all Ag atoms [see Fig. 3(a) and Table I]—seemingly leading to a weak interaction of the Cu atoms with those *far-lying* Ag neighbors, as occurs for Cu atoms in bulk Ag_3Cu and Cu_3Ag alloys. The DOS of Cu atoms in bulk Ag_3Cu [Fig. 7(f)] thus indicates that the strength of the Ag-Cu bond is considerably weak for Cu atoms; in fact, expanding the lattice parameter [Fig. 8(g)] changes insignificantly the DOS of Cu. Second, the effect of the Ag environment on the DOS of Cu atoms in $Ag_{27}Cu_7$ is connected with the depletion of states between 2.5 and 3.5 eV below the Fermi level, i.e., the dip around 3.0 eV in Figs. 7(h), 7(e), and 7(f). We note, in addition, that the DOS of $Ag_{27}Cu_7$ below the dip (~3.5 eV) is remarkably high, as compared to that of bulk alloys [see Figs. 7(f) and 7(g)]—despite the low Cu content—and generates a much stronger hybridization between Cu and Ag states, which is in contrast to that observed in bulk alloys [see Figs. 6(c)–6(e)]. Interestingly, the DOS of Cu atoms at 3.5 eV below the Fermi level in the compressed lattice of bulk Ag_3Cu [Fig. 8(b) is almost as high as that of Cu atoms in $Ag_{27}Cu_7$ and also results in a stronger hybridization between Cu and Ag states as compared to that found in equilibrium bulk Ag_3Cu bulk. Third, we conclude that the *optimum* Cu-Ag bonding in $Ag_{27}Cu_7$ comes about in terms of the electronic DOS through the shortening of Ag-Cu bonds, which allows the hybridization of the *d* states of Cu and Ag atoms, suppressing by this means the dip featuring in the DOS of Cu_3Ag and Ag_3Cu alloys.

Finally, we remark that although the DOS of Ag atoms is not changed as drastically as that of Cu atoms in bulk Ag-Cu alloys—suggesting that Cu is more sensitive than Ag to the chemical environment—the vulnerability of Cu to the presence of Ag is intermixed with long bond-length effects. That is, the presence of Cu depletes the top of the Ag *d*-band as much as Ag depletes the bottom of the Cu *d*-band. However, the short Ag-Ag and Ag-Cu bonds (with respect to bulk Ag), as present in both bulk alloys, broaden the *d*-band of Ag atoms, compensating in this manner the effect of the Cu

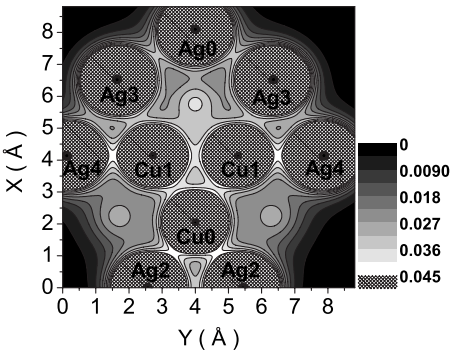

FIG. 10. Two-dimensional (2D) charge density plot at a plane that contains the five-fold rotation axis of the $Ag_{27}Cu_7$ nanoalloy and is, therefore, perpendicular to its mirror plane. Atoms in black color are precisely centered on that plane.

atoms. On the other hand, the Cu-Cu and Cu-Ag bond lengths induced in both bulk alloys never become shorter than that of bulk Cu, rather, it is quite the opposite. As a result the narrowing of the *d*-band of Cu atoms is triggered, aggravating the depletion caused by the presence of Ag atoms and, hence, exaggerating the actual chemical susceptibility of Cu to the Ag environment. In summary, the electronic DOS is found unambiguously related to the bond lengths held in a particular geometry.

If we were to extrapolate the above results to related systems, we would speculate that the dip in the DOS identifies less stable phases of noble metal alloys. For example, based on the patterns found in $Ag_{27}Cu_7$ and the $L1_2$ bulk Ag-Cu alloys, we predict that the stability of Au-Ag alloys and the absence of a dip in their DOS[20] are attributed to the fact that the lattice parameters of bulk Au and Ag are nearly identical and that the *d*-band of bulk Ag lies within that of bulk Au, assuring significant *d*-band hybridization. Likewise, the hybridization between Cu and Au states is strong in bulk Au-Cu alloys because the *d*-band of Cu also lies within that of bulk Au, albeit in the region near its Fermi level, while that of Ag lies deeper. The overlap between the bands of Ag and Cu, on the other hand, is relatively small, resulting in weaker Cu-Ag hybridization in bulk Cu-Ag alloys. The dip in the DOS of Au-Cu is probably not a sign of stability, rather, it may be a sign that structures and/or compositions allowing shorter Au-Cu would be more stable (amorphous phases, perhaps). The heat of formation of bulk Cu_3Au, for example, is nega-

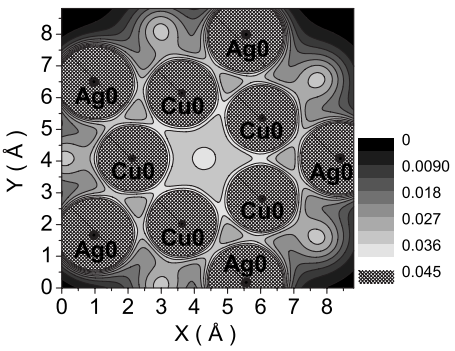

FIG. 11. 2D charge density plot at the mirror plane of $Ag_{27}Cu_7$. Atoms in black color are precisely centered on that plane.

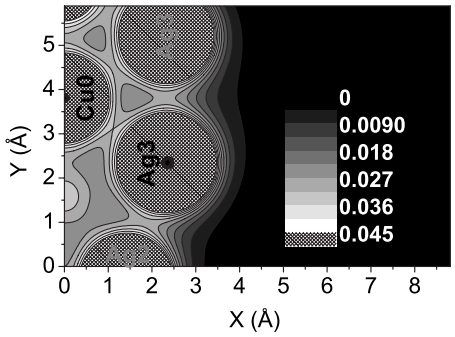

FIG. 12. 2D charge density plot at a plane that contains the positions where Cu0 and Ag3 atoms (black color) are centered. Atoms in gray are depicted in the section but are not centered precisely on that plane.

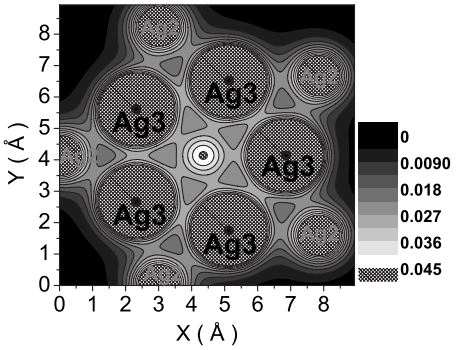

FIG. 14. 2D charge density plot at a plane that is parallel to the mirror plane of $Ag_{27}Cu_7$. The pentagonal layer composed of Ag3 atoms (black color) is contained in this plane. Atoms in gray are depicted in the section but are not centered precisely on that plane.

tive because the strength of the Au-Cu bond is larger than that of bulk Cu and Au, even at the distances dictated by the $L1_2$ phases,[24] but which are not necessarily the distances at which the strength of all three Au-Cu, Au-Au, and Cu-Cu bonds is optimized with the corresponding hierarchal importance, as exemplified by $L1_2$ bulk Ag-Cu alloys, whose long Ag-Cu bonds are in contrast to the significantly short ones found in the $Ag_{27}Cu_7$ nanoalloy.

2. *Charge density distribution of* $Ag_{27}Cu_7$ *nanoalloy*

The first aspect that comes to mind in Figs. 10–15 of the plotted charge densities of the $Ag_{27}Cu_7$ nanoalloy is that Ag atoms barely supply charge to the surface of the nanoalloy. The question is whether the surface charge depletion coincides with charge redistribution from Ag atoms to Cu atoms since two neighboring metals with significantly different work functions can give rise to electron transfer from one metal to the other, as reported in calculations of Pd clusters on Au(111) by Sánchez *et al.*[52] corresponding to a work function difference of ~0.3 eV. Here, the work function of Cu is larger than that of Ag by ~0.2 eV. Indeed, Figs. 10 and 11 display a higher charge density around Cu atoms than around Ag atoms.

The plot of the charge density in a plane passing through ten Ag and Cu atoms in Fig. 10 illustrates that the Cu0-Ag2 and Cu1-Ag4 bonds are linked by the highest bonding charge density, corresponding, indeed, to the shortest Ag-Cu bond lengths (~2.58 Å), implying that they are stronger than the Cu1-Cu1 (2.58 Å) and Cu0-Cu0 (2.58 Å) bonds and even the Cu0-Cu1 bonds (2.55 Å), in that order (see Figs. 10 and 11). The next strength of bonding charge density occurs for Cu0-Ag0 bonds, followed by Cu1-Ag3 bonds, as shown in Figs. 10 and 11. In this case, the bond lengths are 2.72 and 2.73 Å, respectively. Notice that, in the second set of bonds, the charge density is considerably lower than in Cu0-Ag2 and Cu1-Ag4 bonds, which supports the assumption that Ag-Cu interactions die out very rapidly (see Sec. III B 1). The third place in bonding charge density corresponds to Cu0-Ag3 (Fig. 12) bonds and the shortest Ag-Ag bonds: Ag0-Ag3 and Ag2-Ag2 bonds (Fig. 10), whose bond lengths are 2.79, 2.87, and 2.89 Å, respectively (Table I). The first might influence very little Cu0 atoms since the bond is quite large. However, this bonding charge density appears as large as that of Ag0-Ag3, which is 0.1 Å further apart. The next in

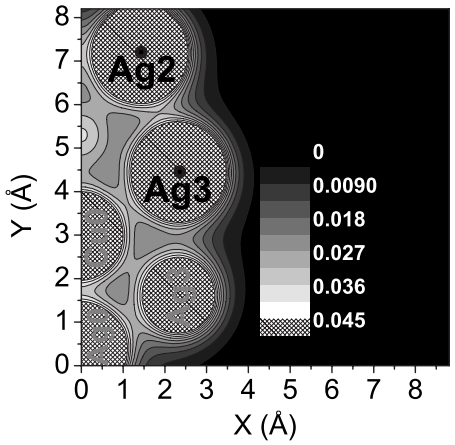

FIG. 13. 2D charge density plot at a plane that contains the positions where Ag2 and Ag3 atoms (black color) are centered. Atoms in gray are depicted in the section but are not centered precisely on that plane.

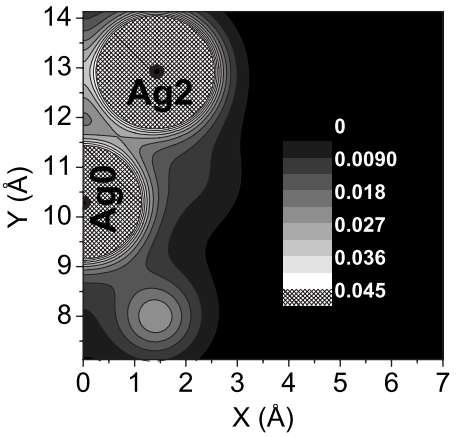

FIG. 15. 2D charge density plot at a plane that contains the positions where Ag0 and Ag2 atoms (black color) are centered. Atoms in gray are depicted in the section but are not centered precisely on that plane.

bonding charge density is the Ag2-Ag3 bond (Fig. 13), whose length is 2.90 Å, followed by the Ag3-Ag4 bond (Fig. 10), whose length is 2.93 Å. The latter bond length is close to that of the Ag0-Ag3 bond (and almost identical to the bond length of bulk Ag); however, the charge density bridging these atoms is slightly weaker. Note that Ag3-Ag3 bonds (Fig. 14) are only slightly longer (2.95 Å), but the bonding charge density around it is less than that around the Ag3-Ag4 bonds. The charge density around the Ag0-Ag2 bond (Fig. 15) is substantially lower than that around Ag3-Ag3, which is consistent with a larger bond length (3.0 Å). The next larger bond lengths are more than ~4 Å, which are expected to provide much weaker direct interactions that will not be discussed here.

In reference to the importance of bond strength and length hierarchies in alloys, as mentioned in Sec. III B 1, we turn to the discussion in Sec. III A 3 of Ref. 39 in which Ag-Ru phonon-stable structures were associated with a high charge density bridging atoms of the same element, whereas phonon-unstable structures were associated with a high charge density bridging atoms of different elements. Instead, following the arguments above, we propose that their charge density plots indicate that Ag-rich structures do not allow for strong Ru-Ru bonds and despite the presence of strong Ru-Ag and Ag-Ag bonds, the structure is unstable. Additional support to our assertion comes from the fact that phonon instabilities are not present in some Ru-rich structures,[39] while those in Ag-rich structures disappear by reducing the equilibrium lattice parameter.[39] Besides, Ag-rich structures with a reduced lattice parameter show clearly that the charge density bridging Ru-Ru bonds is enhanced [see Fig. 3(e) of Ref. 39]. The above discussion suggests that in Ag-Ru alloys, the strength hierarchy is in the following order: {Ru-Ru, Ag-Ru, Ag-Ag}. In fact, relatively large differences between the strength of Ru-Ru and Ag-Ru bonds and a pronounced deep dip in the DOS can be expected to explain all their results simultaneously.

IV. SUMMARY

We have presented DFT calculations of the $Ag_{27}Cu_7$ nanoalloy to understand its structure and relative stability via considerations of its energetics, electronic DOS, and charge density distribution. The local coordination of Cu atoms is similar to that of bulk Cu regarding the number of first and second NNs, whereas Ag atoms find themselves in a low-coordinated environment and, in exchange, form Ag-Cu bonds which are as short as the shortest Cu-Cu bonds. On the other hand, the electronic structure of the Cu atoms in $Ag_{27}Cu_7$ deviates much more from that of atoms in bulk Cu, as compared to the corresponding case of Ag atoms in this nanoalloy.

Related bulk alloys, Ag_3Cu and Cu_3Ag, are found to have a positive heat of formation and form bonds larger than the shortest ones found in the $Ag_{27}Cu_7$. However, we find that the resulting interatomic bonds in these bulk alloys are sufficiently strong such that their cohesive energy is larger than that of bulk Ag and their phonon dispersion curves do not display instabilities.

From our analyses of the geometric and electronic structures, we conclude that the relative stability of $Ag_{27}Cu_7$, among its nanoalloy family, is a result of the maximization of the number of Cu-Cu and Cu-Ag bonds, using the minimum number of Cu atoms. The core-shell Ag-Cu nanoalloys do not behave differently from the corresponding bulk alloys regarding segregation tendencies and migration of Ag to the surface, as pointed earlier,[54] since $Ag_{27}Cu_7$ is segregated by construction. Furthermore, the segregated structure is the attribute that leads to its relative stability, provided the core-shell structure allows the formation of strong Cu-Cu and Cu-Ag bonds without contracting the typical Ag-Ag bond or (most importantly) stretching the typical Cu-Cu bond.

The HOMO-LUMO gap of $Ag_{27}Cu_7$ is found to be 0.77 eV. The DOS of $Ag_{27}Cu_7$ shows features similar to those of the Ag-Cu bulk alloys. We find that the additional features of the DOS of fully coordinated Cu atoms in $Ag_{27}Cu_7$ are caused by the relatively long distance separating Cu atoms from half of its first NN. Short Ag-Cu bond lengths, on the other hand, improve the hybridization of Cu and Ag states, explaining why the hybridization of Cu and Ag states in the $Ag_{27}Cu_7$ nanoalloy is stronger than in Ag-Cu bulk alloys. The observed differences in electronic DOS between $Ag_{27}Cu_7$ and $L1_2$ alloys arise not only because of low coordination and geometry differences but mainly because the symmetry enforces long Cu-Cu and Cu-Ag bonds, unlike the situation in $Ag_{27}Cu_7$.

In $Ag_{27}Cu_7$, the charge density along Ag-Cu bonds, whose length is ~2.6 Å, is even larger than that around Cu-Cu bonds and certainly larger than that bridging Ag-Ag atoms. Nevertheless, Ag-Cu bonds whose length is of the order of that in bulk Ag_3Cu, or even Cu_3Ag, are surrounded by an appreciably quenched charge density, explaining why the DOS of Cu atoms show low coordination features.

We infer a hierarchy of bond strength intrinsic to Cu and Ag: {Cu-Cu > Cu-Ag > Ag-Ag}. The nanoalloy structures that enforce such a hierarchy also obey a bond-length order {Ag-Ag > Cu-Ag > Cu-Cu}. Clearly, the strength and length of the bonds are correlated properties in any particular structure. Hence, for a given composition of a nanoalloy, the global-minimum structure will be that which simultaneously maximizes the number of the strongest bonds while maintaining the bond-length order and, thus, fulfilling the bond strength hierarchy that ultimately minimizes the energy.

ACKNOWLEDGMENTS

We are indebted to Riccardo Ferrando for providing us with the initial configuration of the $Ag_{27}Cu_7$ nanoalloy. This work was supported in part by DOE under Grant No. DE-FG02-03ER46058.

*alcantar@physics.ucf.edu
†talat@physics.ucf.edu

[1] G. Rossi, A. Rapallo, C. Mottet, A. Fortunelli, F. Baletto, and R. Ferrando, Phys. Rev. Lett. **93**, 105503 (2004).
[2] T. Shibata, B. A. Bunker, Z. Zhang, D. Meisel, C. F. Vardeman II, and J. D. Gezelter, J. Am. Chem. Soc. **124**, 11989 (2002).
[3] S. Darby, T. V. Mortimer-Jones, R. L. Johnston, and C. Roberts, J. Chem. Phys. **116**, 1536 (2002).
[4] E. Cottancin, J. Lermé, M. Gaudry, M. Pellarin, J. L. Vialle, M. Broyer, B. Prével, M. Treilleux, and P. Mélinon, Phys. Rev. B **62**, 5179 (2000).
[5] H. Portales, L. Saviot, E. Duval, M. Gaudry, E. Cottancin, M. Pellarin, J. Lermé, and M. Broyer, Phys. Rev. B **65**, 165422 (2002).
[6] S. Giorgio and C. R. Henry, Eur. Phys. J.: Appl. Phys. **20**, 23 (2002).
[7] M. Moskovits, I. Srnová-Šloufová, and B. Vlčková, J. Chem. Phys. **116**, 10435 (2002).
[8] H. Tada, F. Suzuki, S. Ito, T. Akita, K. Tanaka, T. Kawahara, and H. Kobayashi, J. Phys. Chem. B **106**, 8714 (2002).
[9] M. Valden, X. Lai, and D. W. Goodman, Science **281**, 1647 (1998).
[10] L. M. Molina and B. Hammer, Phys. Rev. Lett. **90**, 206102 (2003).
[11] M. Haruta, Catal. Today **36**, 153 (1997).
[12] A. Sanchez, S. Abbet, U. Heiz, W. D. Schneider, H. Hakkinen, R. N. Barnett, and U. Landman, J. Phys. Chem. **103**, 9573 (1999).
[13] B. Huber, P. Koskinen, H. Häkkinen, and M. Moseler, Nat. Mater. **5**, 44 (2006).
[14] S. Lee, C. Fan, T. Wu, and S. L. Anderson, J. Chem. Phys. **123**, 124710 (2005).
[15] P. Jensen, Rev. Mod. Phys. **71**, 1695 (1999).
[16] C. Ashman, S. N. Khanna, F. Liu, P. Jena, T. Kaplan, and M. Mostoller, Phys. Rev. B **55**, 15868 (1997).
[17] K. Kokko, E. Ojala, and K. Mansikka, J. Phys.: Condens. Matter **2**, 4587 (1990).
[18] J. P. K. Doye and F. Calvo, Phys. Rev. Lett. **86**, 3570 (2001).
[19] B. von Issendorff and O. Cheshnovsky, Annu. Rev. Phys. Chem. **56**, 549 (2005).
[20] K. Terakura, T. Oguchi, T. Mohri, and K. Watanabe, Phys. Rev. B **35**, 2169 (1987).
[21] J. M. Sánchez, J. P. Stark, and V. L. Moruzzi, Phys. Rev. B **44**, 5411 (1991).
[22] A. van-de Walle and G. Ceder, Rev. Mod. Phys. **74**, 11 (2002).
[23] R. Heid and K. P. Bohnen, Phys. Rep. **387**, 151 (2003).
[24] Illustrations can be found at http://cst-www.nrl.navy.mil/lattice/ as provided by the Center for Computational Materials Science of the United States Naval Research Laboratory.
[25] R. O. Jones and O. Gunnarson, Rev. Mod. Phys. **61**, 689 (1989).
[26] S. Baroni *et al.*, Complete Quantum-ESPRESSO, Distribution Version 3.0, 2005, http://www.pwscf.org.
[27] D. Vanderbilt, Phys. Rev. B **41**, 7892 (1990).
[28] J. P. Perdew, K. Burke, and M. Ernzerhof, Phys. Rev. Lett. **77**, 3865 (1996).
[29] M. Methfessel and A. T. Paxton, Phys. Rev. B **40**, 3616 (1989).
[30] H. J. Monkhorst and J. P. Pack, Phys. Rev. B **13**, 5188 (1976).
[31] S. Baroni, P. Giannozzi, and A. Testa, Phys. Rev. Lett. **58**, 1861 (1987).
[32] P. Giannozzi, S. de Gironcoli, P. Pavone, and S. Baroni, Phys. Rev. B **43**, 7231 (1991).
[33] D. K. Blat, N. E. Zein, and V. I. Zinenko, J. Phys.: Condens. Matter **3**, 5515 (1991).
[34] K. H. Hellwege and A. M. Hellwege, in *Condensed Matter*, edited by K. H. Hellwege and A. M. Hellwege, Landolt-Börnstein, New Sereis, Vol. 2 Group III (Springer-Verlag, Berlin, 1969).
[35] In order to take advantage of the plane wave approach, the nanoalloy is modeled in a periodic supercell, which is large enough so as to minimize the interactions between neighboring $Ag_{27}Cu_7$, clusters by reducing the overlap between the wave functions of neighboring clusters. Valence electrons are thus confined spatially in the cluster, implying that electrons in each level specified by an index band n, and wave vector $\boldsymbol{k}$, have a vanishing mean velocity given by $\boldsymbol{v}_n(\boldsymbol{k})=\frac{1}{\hbar}\boldsymbol{\nabla}_{\boldsymbol{k}}\epsilon_n(\boldsymbol{k})\rightarrow 0$ (Ref. 55), implying that the electronic bands $\epsilon_n(\boldsymbol{k})$, are constant over the BZ. It is thus safe to assume that one k point (any) is sufficient to accurately perform the calculation and that no additional information will be obtained by sampling the BZ. To confirm the above, we performed total energy calculations of $Ag_{27}Cu_7$, with 1, 8, and 24 special k points to find that the total energy changes by only 4×10^{-5} eV, while forces on each atom remain below 8×10^{-3} eV/Å. Furthermore, non-self-consistent calculations at 24 k points were performed and showed that the band structure of $Ag_{27}Cu_7$ is a set of flat bands (see Fig. 5).
[36] A. DalCorso, Phys. Rev. B **64**, 235118 (2001).
[37] G. Cipriani, D. Loffreda, A. Dal-Corso, S. de-Gironcoli, and S. Baroni, Surf. Sci. **501**, 182 (2002).
[38] R. Ferrando (private communication).
[39] Y. Kong, J. H. Li, L. T. Kong, and B. X. Liu, Phys. Rev. B **72**, 024209 (2005).
[40] J. H. He, H. W. Sheng, J. S. Lin, P. J. Schilling, R. C. Tittsworth, and E. Ma, Phys. Rev. Lett. **89**, 125507 (2002).
[41] J. H. He, H. W. Sheng, P. J. Schilling, C. L. Chien, and E. Ma, Phys. Rev. Lett. **86**, 2826 (2001).
[42] B. X. Liu, W. S. Lai, and Z. J. Zhang, Adv. Phys. **50**, 367 (2001).
[43] E. Peiner and K. Kopitzki, Nucl. Instrum. Methods Phys. Res. B **34**, 173 (1988).
[44] A. Kara and T. S. Rahman, Surf. Sci. Rep. **56**, 159 (2005).
[45] P. D. Bogdanoff, B. Fultz, and S. Rosenkranz, Phys. Rev. B **60**, 3976 (1999).
[46] P. K. Sharma and N. Singh, Phys. Rev. B **4**, 4636 (1971).
[47] M. Schmidt, R. Kusche, B. von Issendorff, and H. Haberland, Nature (London) **393**, 238 (1998).
[48] U. Hild, G. Dietrich, S. Krückeberg, M. Lindinger, K. Lützenkirchen, L. Schweikhard, C. Walther, and J. Ziegler, Phys. Rev. A **57**, 2786 (1998).
[49] H. Yildirim, K. Kara, and T. S. Rahman (unpublished).
[50] The thermodynamics of finite quantum-mechanical interacting systems depends on the number Γ—as a function of the energy E, number of particles N, and volume V—of distinct eigenstates of the Hamiltonian of the system that render a total energy $E'=E\pm\Delta$, where $\Delta\ll E$. The configurational entropy is then given by $S_{conf}=k_B\ln(\Gamma)$. While obtaining the exact solution of the interacting Hamiltonian is a formidable task, we can obtain $S_{conf}(\Gamma)$ directly for an interacting bimetallic N-atom cluster $X_{N1}Y_{N-N1}$. Namely, the total energy and the electronic structure of an $X_{N1}Y_{N-N1}$ cluster are defined by the geometric configuration of its nuclei and, hence, different geometric configurations of the atoms define distinct eigenstates that may or may not be

degenerate. We can thus straightforwardly say that a cluster $X_{N1}Y_{N-N1}$, with m degenerate isomers will have a configurational entropy $S_{conf}=k_B \ln(m)$. Rossi *et al.*, using tight binding many-body potentials in combination with the GGO method, found that the total energy of the next-lowest-energy isomer has a total energy 0.3 eV higher than that of $Ag_{27}Cu_7$. DFT, in turn, finds that such an isomer has an energy 0.8 eV higher than that of $Ag_{27}Cu_7$. Therefore, in this case, we may assume that $Ag_{27}Cu_7$ has no degenerate isomers and so its S_{conf} is zero. For the other clusters in this family, however, a similar investigation of the isomers has to be performed, keeping in mind that even for doubly degenerate isomers ($m=2$), configurational entropic contributions to the free energy of $TS_{conf}=18$ meV ($T=300$ K) will arise and give rise to clusters with a free energy lower than that of $Ag_{27}Cu_7$, at room temperature.

[51] K. Kokko, J. Phys.: Condens. Matter **11**, 6685 (1999).

[52] C. G. Sánchez, E. P. M. Leiva, and W. Schmickler, Electrochem. Commun. **5**, 584 (2003).

[53] G. K. Wertheim, S. B. DiCenzo, and D. N. E. Buchanan, Phys. Rev. B **33**, 5384 (1986).

[54] F. Baletto, C. Mottet, and R. Ferrando, Eur. Phys. J. D **24**, 233 (2003).

[55] N. W. Ashcroft and N. D. Mermin, *Solid State Physics*, 1st ed. (Thomson Learning, 1976).